Effects of geomagnetic mirror force and pitch angles of precipitating electrons on ionization of the polar upper atmosphere

Tomotaka M. Tanaka^{1,2}, Yasunobu Ogawa^{1,2}, Yuto Katoh³, Mizuki Fukizawa², Anton Artemyev⁴, Vassilis Angelopoulos⁴, Xiao-Jia Zhang⁵, Yoshimasa Tanaka^{1,2,6}, Akira Kadokura^{2,6}

¹The Graduate University for Advanced Studies, SOKENDAI, Japan

Correspondence to: Tomotaka Tanaka (tanaka.tomotaka@nipr.ac.jp)

Abstract. We studied the effects of the geomagnetic mirror force on electron density enhancements in the polar atmosphere due to energetic electron precipitation. Using the pitch angle and energy distribution of electrons observed by the low-altitude Electron Losses and Fields INvestigation (ELFIN) satellites as initial conditions, the electron density in the atmosphere caused by precipitating electrons was calculated usingby a simulation with two different methods: a traditional method that does not include the effect of the mirror force and a recently developed method that includes the effect. From a simultaneous observation event of the ELFIN satellite and the European Incoherent SCATter scientific radar system (EISCAT) Tromsø radar, it was found that the method with the effect of the mirror force reduces electron density by about 40% at an altitude of 80 km compared to the traditional method. This decrease was pronounced-when the pitch angle distribution of high-energy electrons was concentrated in the pitch angle range of the trapped component and near the loss conewhen the pitch angle distribution of high energy electrons was concentrated in the trapped and boundary regions. The maximum decrease was 50%. For an event where the altitude profile of electron density was accurately determined from the EISCAT radar, the electron density profile estimated using the method with the effect of mirror force showed betterIt was verified that electron density distribution estimated using the method with the effect of mirror force showed good agreement with anthe electron density profile derived from the EISCAT radar. The validation comparison of between simulation results based on and these observation data contributes to the establishment and improvement of atmospheric ionization models using various types of precipitating electrons.

1 Introduction

The energetic (> 50 keV) electron precipitation (EEP) has attracted attention due to its impact on mesospheric ionization and ozone chemistry. It has been focused on the impact of energetic electron (> 50 keV) precipitation (EEP) on the ozone. Miyoshi

²National Institute of Polar Research, NIPR, Japan

³Tohoku University, Japan

⁴University of California, Los Angeles, UCLA, United States of America

⁵University of Texas, Dallas, UTD, United States of America

O Goint Support-Center for Data Science Research, ROIS, JAPAN

et al. (2020) suggested that precipitating energetic electrons penetrate to lower altitudes with the appearance of diffuse auroras. Ovama et al. (2017) reported electron density enhancements in the lower D-region ionosphere during pulsating auroral events. attributed to EEP. Because the energetic electrons maintain high energy even after passing through the auroral altitude, they have been found to cause electron density enhancement at about 50 km altitude (Oyama et al., 2017). These enhancements may accelerate chemical reactions and the production generation of nitrogen or hydrogen oxides, which to destroy ozone in the mesosphere below 80 km altitude (Turunen et al., 2016). Thus, it has been suggested that EEP has ability to make chemical changes in the lower altitude based on both observations and simulation (Miyoshi et al., 2021; Ozaki et al., 2022; Murase et al. 2022). However, modeledthe ionization rates due toby EEP can differ by between models up to an order (Nesse et al., 2022). Therefore, it is necessary to evaluate the effects of EEP on the atmosphere accurately by considering simulation improvements. The mirror force, one of the effects of the magnetic field on the charged particles, has recently been considered in numerical simulations of atmospheric ionization by precipitating electrons. As the magnetic field strength at atmospheric altitudes is nearly constant, the change in the pitch angle of precipitating electrons by the effect of the mirror force has been considered negligible (Rees, 1963). Even if some numerical simulations included the pitch angle, it was only used to calculate the altitude change of the electron motion using the inclination of the magnetic field and pitch angle. Thus, velocity changes due to the mirror force were still ignored (Solomon, 1993, 2001). A Recently, a numerical simulation to calculate the altitude profile of atmospheric ionization rate by EEP, including the effect of the mirror force, was developed (Lehtinen et al., 1999), and the results of the simulation were parameterized by the pitch angle and energy of the electron (Xu et al., 2020). Furthermore, using a newly developed simulation, Katoh et al. (2023) showed the concrete difference in ionization rates between cases with and without the effect of the mirror force. By comparing the simulation results with and without the effect, it was found that when an electron with a large pitch angle had energies above 100 keV, the ionization rate of the former was less than 10% of the latter (Katoh et al., 2023). However, this effect has not yet been verified or confirmed by any observational data. However,

Although some satellites have observed electrons." energy and pitch angle distribution, it has been challenging to use them in the simulation as input. The Arase satellite, for example, is too far away to observe the pitch angle distribution of electrons reaching the earth's atmosphere in detail, while the energy range of electrons observed by the Reimei satellite was too low to make differences between cases between with and without the effect of the mirror force, as shown in Katoh et al. (2023). However, the ELFIN (Electron Losses and Fields Investigation CubeSats) satellites, a-polar-orbiting and low-altitude satellites, observed both pitch angle and energy distribution of energetic electrons. Therefore, it has been possible to evaluate the actual atmospheric effects by combining the satellites with the simulations developed by Katoh et al. (2023).

50

65

actual data has not yet confirmed this.

This study aims to evaluate the effect of the mirror force on atmospheric electron density <u>integratingusing the</u>-satellite <u>observations withand the</u> simulation <u>resultss</u> and <u>subsequently validating to validate</u> the results <u>withusing the</u> radar <u>data</u>. Even though it is challenging to evaluate the ionization rate, calculating the electron density from the ionization rate enabled us to compare it with observational data. Using the pitch angle and energy distributions of electrons observed by the ELFIN (Electron Losses and Fields INvestigation CubeSats) satellites, we calculated the electron density enhancement due to the

precipitating electrons with and without the effect separately to compare them with the actual data observed by the EISCAT (European Incoherent Scatter) Tromsø radar. In this study we mainly show comparison results with simulations focusing on the event of December 16, 2021, when the altitude profile of electron density was obtained accurately from EISCAT observations.

2 Methods and Instruments

2.1 ELFIN satellites

70

75

85

We used data from the ELFIN satellites. The satellites wereas launched in September 2018 and completed observations in September 2022. They were on a low-altitude (~450 km altitude) polar orbit (~93° inclination), and the orbital period is about 90 min. It consists of two CubeSats (ELFIN-A/B), flying in nearly identical orbits with a time difference of less than 20 min (Angelopoulos et al., 2020). Each satellite had an energeticy particle detector for electrons (EPDE), which measured 50 – 7000 keV electrons with $\Delta E/E < 40\%$ energy resolution and 22.5° pitch angle resolution. Since the electron flux above 2500 keV is negligible compared to electrons with energies below that, we used the electron flux data between 50 and 2500 keV in this study. The spin axis is kept perpendicular to the orbital plane, and the whole pitch angle is observed twice every spin period (~2.85 s) (Zhang et al., 2022). A loss cone angle θ_{LA} is defined as a equation

$$\theta_{L.A.} = \sin^{-1} \sqrt{\frac{B}{B_{100}}} \tag{1}$$

where *B*, and *B*₁₀₀ are the magnetic field strength at the satellite location and at 100 km altitude, respectively. In other words, it is the maximum pitch angle of electrons at the satellite point which can enter the atmosphere below 100 km altitude while moving in the magnetic field. The IGRF model (Alken et al., 2021) was used as a magnetic field model to calculate the loss cone angle. The loss cone angle was defined as the angle at which the pitch angle would be 90 degrees at 100 km altitude if an electron moves with the Lorentz force due to the geomagnetic field.

2.2 EISCAT UHF/VHF Tromsø radar

We also used the EISCAT Tromsø UHF radar₂, which has been in operation since 1981 at Tromsø (69.6°N, 19.2°E, and magnetic latitude of 66.2°) in northern Scandinaviahas been operated in Northern Scandinavia since 1981 and in Svalbard since 1996. This radar One of the radars is located at Tromsø (69.6°N, 19.2°E, and magnetic latitude of 66°), which observes the altitude profile of electron density and other ionospheric parameters (Folkestad, K., 1983). For all events in this study, the beata pulse code was utilized, and the beam was directed along to the magnetic field line. The electron density data used in this study were obtained with the beam aligned along the magnetic field lines, and were derived from the power profile data using the standard analysis software GUISDAP (Lehtinen and Huuskonen, 1996). Appropriate power calibration was

performed by comparing the radar-derived electron densities with the co-located ionosonde measurementss (foF2, and foE) or model estimates (pline), and calibration factors were applied accordingly.

2.3 Simulation

95

100

105

110

115

120

125

The simulation used in this study is a Monte Carlo simulation developed by Katoh et al. (2023). It has atmospheric data of oxygen atoms, oxygen molecules, and nitrogen molecules using the NRLMSIS 2.1 emprical modepymsis model (Lucas, 2022; Emmert et al., 2020; Emmert et al., 2022; Pieone et al., 2002; Celestrak; Matzka et al., 2021). It enables us to calculate the altitude profile of the ionization rate above Tromsø (L=6.45), using the data of an electron precipitating electron parameters initial conditions—such as altitude, pitch angle, and energy—as initial conditions. The effect of the Lorentz force can be included or excluded manually when calculating particle transport. When considering the force, the magnetic field at a distance of Larmor radius from the magnetic field line leading to Tromsø was given to satisfy $\nabla \cdot \mathbf{B} = 0$ and used in the calculations (see Katoh et al., 2023).

2.4 Combination of the ELFIN satellites data and the simulation

First, we searched for events in which either of the ELFIN satellites approached the EISCAT Tromsø radar. We used the IGRF model to calculate the geomagnetic footprints of the satellite, and selected events in which, which was defined as the situation in which the geomagnetic latitude was within coordinate of the satellite was in the region $69.6^{\circ}N \pm 2^{\circ}$, and the longitude was within 19.2°E ± 5°. Second, we selected events that showed some electron density peak under 100 km altitudes or had a density of more than 10¹⁰ m⁻³ at 85 km altitude in the EISCAT data, which should be caused by the EEP. Next, we used the differential number flux of electrons data in each energy and pitch angle energy bin observed by the ELFIN satellite as the initial condition of the simulations. For each bin, we simulated to ealeulate the altitude profile of collision rate $R [m^{-1}]$, defined as that is, the number of ionization events produced by a single precipitating electron in each 1 m altitude interval made in the atmosphere. For some specific bins containing the loss cone angle, the collision rate was calculated more precisely by dividing the pitch angle range of the bin into ten parts and averaging the results. Katoh et al. (2023) described the method for calculating the collision rate and demonstrated that it varies sensitively with pitch angle near the loss cone angle. -during its 1 m movement at the altitude. The observed differential number flux f [s⁻¹m⁻²str⁻¹MeV⁻¹] was integrated over the observed energy and pitch angle range to obtain the total number flux $F[s^{-1}m^{-2}]$ for each bin. Then, each R profile, representing the collision rate, was multiplied by the corresponding total number flux F to calculate the ionization rate profile for that bin. The ionization rates from all bins were finally summed to obtain the total ionization rate $O[s^{-1}m^{-3}]$ as a function of altitude. For some specific bins containing the loss cone angle, the collision rate was calculated more precisely. In other words, we divided the pitch angle range of the bin into ten parts to simulate separately, and we averaged these ten results. This is because simulation results near the loss cone angle vary significantly depending on the initial pitch angle. The results of each simulation were integrated depending on the observed range of energy and pitch angle. The differential number flux f [stMe] observed by the satellite was integrated according to the observed range of energy and pitch angle to obtain the total number flux F []. It was multiplied by R to obtain the ionization rate Q. The electron density is estimated from the rate Q using the following method. The time variation of the electron density N_e [m⁻³] due to production and recombination is

$$\frac{\mathrm{d}N_e}{\mathrm{d}t} = Q - \alpha N_e^2 \tag{2}$$

where α [m³s⁻¹] is an effective recombination rate proposed byef Gledhill (1986), and] is the electron density. This recombination rate is a statistical estimate derived from electron density measurements during auroral events. Although image data were not always available due to bad weather conditions, electron density enhancements were clearly identified in the auroral emission altitude region. Therefore, it is reasonable to apply this value of the recombination rate in the present analysis. Since As the time variation of electron density can be assumed to be negligible compared to smaller than the time resolution of the observations, i.e., dNe dt ≈ 0-, we got the electron density was calculated as Ne = √2/α. Then, the altitude profile of electron density was calculated both with and without consideration of the effect of the mirror force. The ratio of the density with the mirror force effect to that without the force effect at 80 km altitude is used as a metric measure of the mirror force effect, and we refer to this as, hereinafter, is called the "density ratio." We showed the density ratios at an altitude of 80 km as representative values in this paper. Finally, a comparison was made between simulations and observations of the altitude profile of electron density during the 15 seconds when the footprint of the satellite and the radar weare closest.

3 Results

145

150

155

3.1 Event on December 16, 2021

3.1.1 Event summery

There were fourive events in whichthat the ELFIN satellite and the EISCAT Tromsø radar observed simultaneously, and the electron density increased under 100 km altitude. Especially in the event on December 16, 2021, at about 07:14 UT, the satellite footprint was the closest to the radar, and they were thought to be under simultaneous observation of an electron density enhancement in the atmosphere caused by EEP. In this event, the *AE* index was up to 300 nT, and geomagnetic pulsations were found. The solar wind was quiet, with Bz at -2 nT and SYM-H at -16 nT. Figure 1 shows the footprints of the ELFIN-A for about 5 min from around 07:12 UT and the location of the EISCAT Tromsø radar. The satellite traveled southward and was closest to the radar around 7:14:30 UT. The red dots show the satellite position during the 15 seconds for which we used the observation data in this study.

Figure 2a shows that the EISCAT Tromsø radar data observed electron density enhancement with that athe value was more than 2×10^{10} m⁻³ for 10 min and that it had double peaks when the satellite was the closest to the radar, one was at 104.8 km altitude, and the other was at 94.7 km altitude in the electron density profile. It is assumed that an EEP observed by the satellite made the second peak. Figure 2b shows that the electrons have a wide range of pitch angles, from small angles up to 90 degrees,

and tend to be close to isotropice isotropic pitch angle distribution of electrons in the north of the radar, while most of the electrons had larger pitch angles than the loss cone angle at the southern range. It was also observed in Fig. 2c that most of the energetic electrons above 500 keV had were with large pitch angles, regardless of location. Figures 2d and 2e show that at the closest approach time, electrons with energy above 1000 keV were observed and that trapped electrons were the majority above 100 keV. Figure 2f shows the fraction of energy flux of precipitating, boundary, and trapped electrons separately among electrons with energy between 50 and 2500 keV. Note that the "boundary electrons" are defined as electrons observed in bins of the EPDE instrument in the satellite equipment whose observation range includes the loss cone angle. Figure 2g is the density ratio at 80 km altitude, and Fig. 2h is the location of the ELFIN satellite. The time range in Figs. 2f and 2g isare restricted between 07:13 and 07:16 because the number of electrons observed by the satellite at other times was not enough to be analyzed meaningfully. These three figures were compared in order to investigate trends in the density ratio. The density ratio decreased as the satellite went south; that is, the L-value and the invariant latitude got smaller, and simultaneously, the ratio of trapped and boundary electrons became larger. For example, the density ratio was 0.8 at maximum when the trapped electrons occupied about half of the energy flux at the location with the L-value of 10 and the invariant latitude of 72°. On the other hand, the value was 0.5 at minimum when the L-value was five, and the invariant latitude was 63°. The trapped and boundary electrons were responsible for more than 75% of the total energy flux. The density ratio was especially 0.6 at the point where the footprint of the ELFIN satellite was the closest to the radar. In other words, we can say that the density ratio became smaller as the electrons with large pitch angles were more dominant in the distributions.

160

165

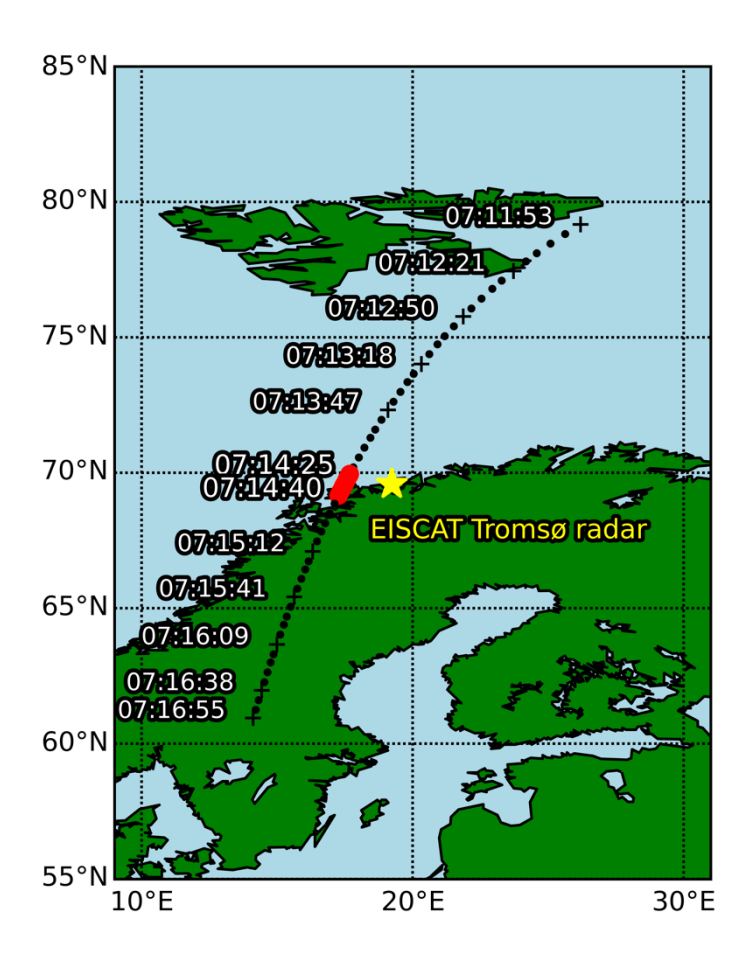
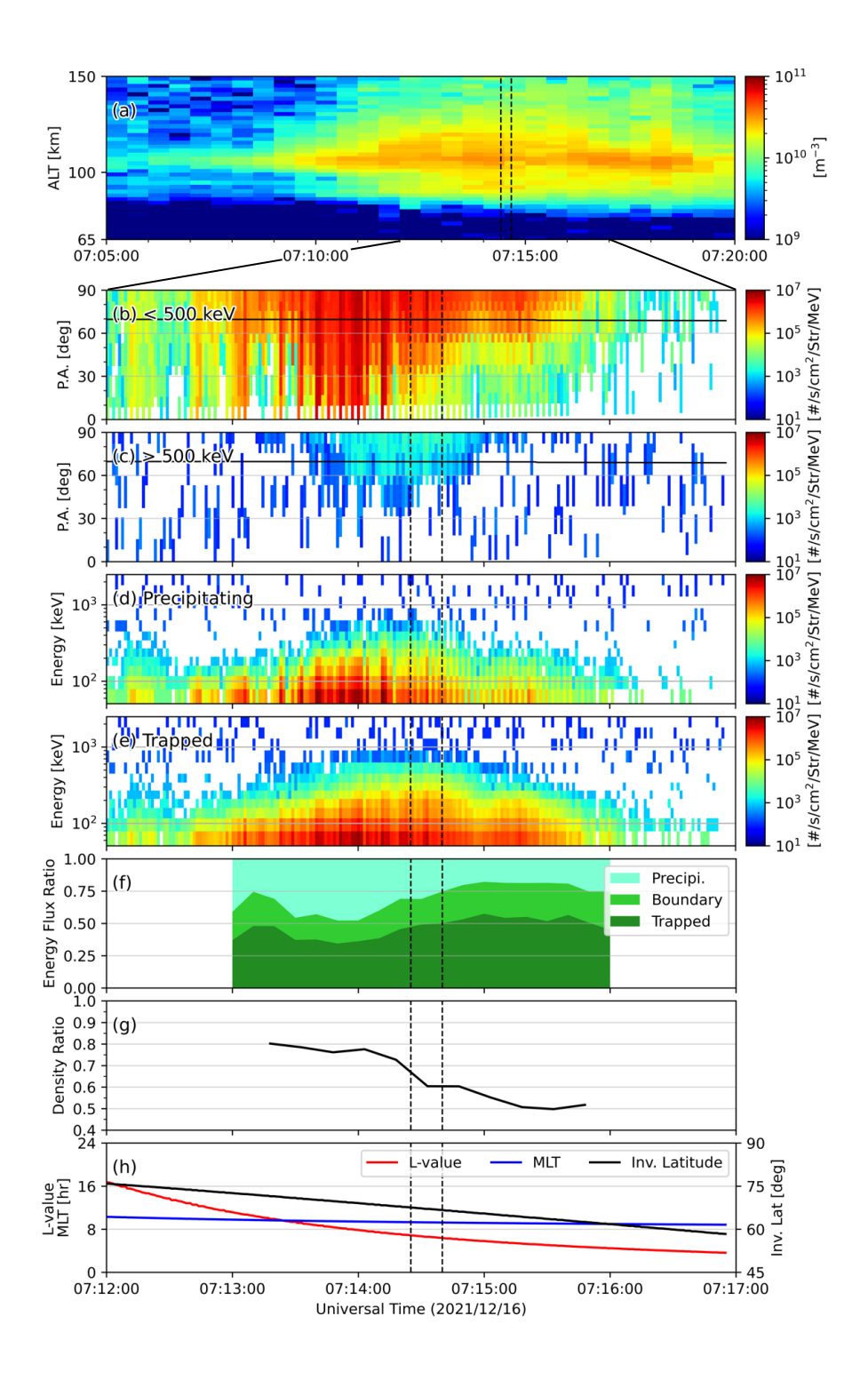


Figure 1: The footprint of the ELFIN satellite (black and red dots) and the location of the EISCAT Tromsø radar (yellow star). The red ones show the satellite footprint for 15 s when both were the closest during the event.



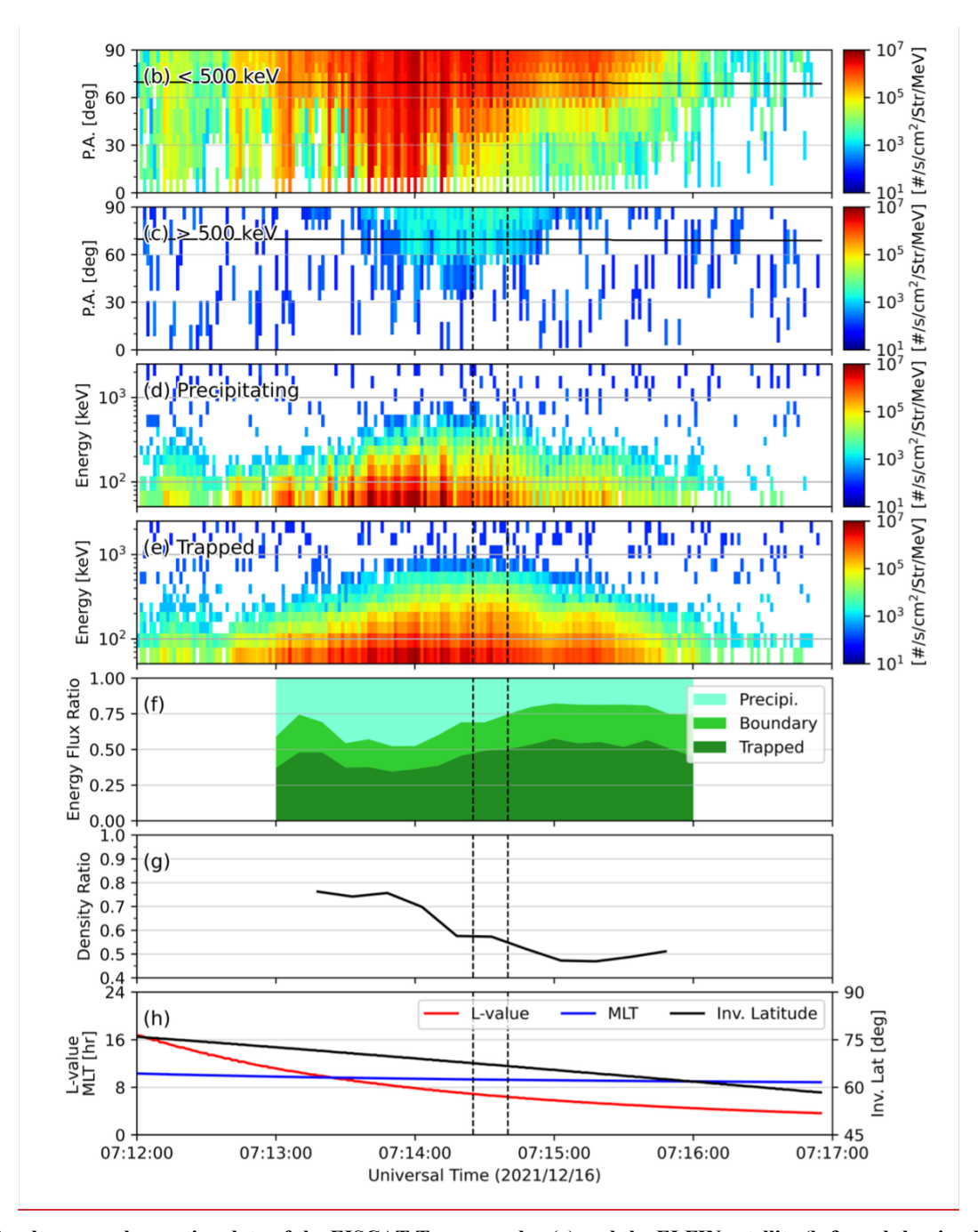


Figure 2: Simultaneous observation data of the EISCAT Tromsø radar (a) and the ELFIN satellite (b-f), and the simulation result (g). (a) Altitude profile of electron density observed by the EISCAT. (b) Average pitch angle distributions of the electron number flux below 500 keV were observed by the satellite. (c) Same as (b) but for that above 500 keV. (d) Average energy distributions of the electrons with the pitch angles less than the loss cone angle. (e) Same as (d) but for those more than the loss cone angle. (f) Fraction of the energy flux for precipitating, boundary, and trapped electrons. (g) The density ratio at 80 km altitude from the

simulations with/without mirror force effect. (h) Information on the geomagnetic location of the satellite: L-value, magnetic local time, and invariant latitude. Two vertical dashed lines show the 15 s time span of the closest approach of the satellite to the EISCAT, corresponding to the red dots in Fig. 1.

3.1.2 Data of the ELFIN satellite

190

195

200

205

Figure 3 shows the pitch angle and energy distribution of the electron number flux observed by the ELFIN satellite. The time range of Fig. 3(b) includes the time of closest approach of the satellite to the EISCAT Tromsø radar. As mentioned in the introduction, the effect of the mirror force is essential mainly for electrons with large pitch angles and with energy more than 100 keV. According to Fig. 3(b), most electrons with energy less than 1000 keV had large pitch angles, though the pitch angle distribution of electrons with higher energy than 1000 keV did not show any apparent tendencies. Specifically, the number flux of electrons with 63 keV electrons, for example, was about 10⁶ s⁻¹cm⁻²str⁻¹MeV⁻¹ with a pitch angle larger than 70° while that was less than 10⁵ s⁻¹cm⁻²str⁻¹MeV⁻¹ with a pitch angle less than 30°. The analysis for the entire observed energy range revealed that the electrons with pitch angles almost equal to or greater than the loss cone angle account for about 72% of the total energy flux.

The distributions in Figs. 3(a) and 3(c) are the same as in Fig. 3(b) except for observation time, which has time ranges of 150 s before and after the time of Fig. 3(b). Teven though hese ELFIN satellite observations suggest that the trapped particles became slilghtly more dominant for lower-energy electrons (Sergeev et al., 2012). However, the electron density measurement by the EISCAT radar consistently shows the second peak of enhancement at around 95 km altitude (see Fig. 2(a)), which corresponds to tens-of-keV electrons at least according to the stopping height (Turunen et al., 2009). Therefore, although the satellite did not pass through just above the radar, it is reasonable to consider the comparison at the time of closest approach to be meaningful, since both instruments were likely observing precipitating electrons in a common energy range, and the resulting ionization profiles are comparable, it can be estimated that electrons should have a similar distribution above the radar because the distribution was almost the same in a wide area, as shown in Fig. 3.

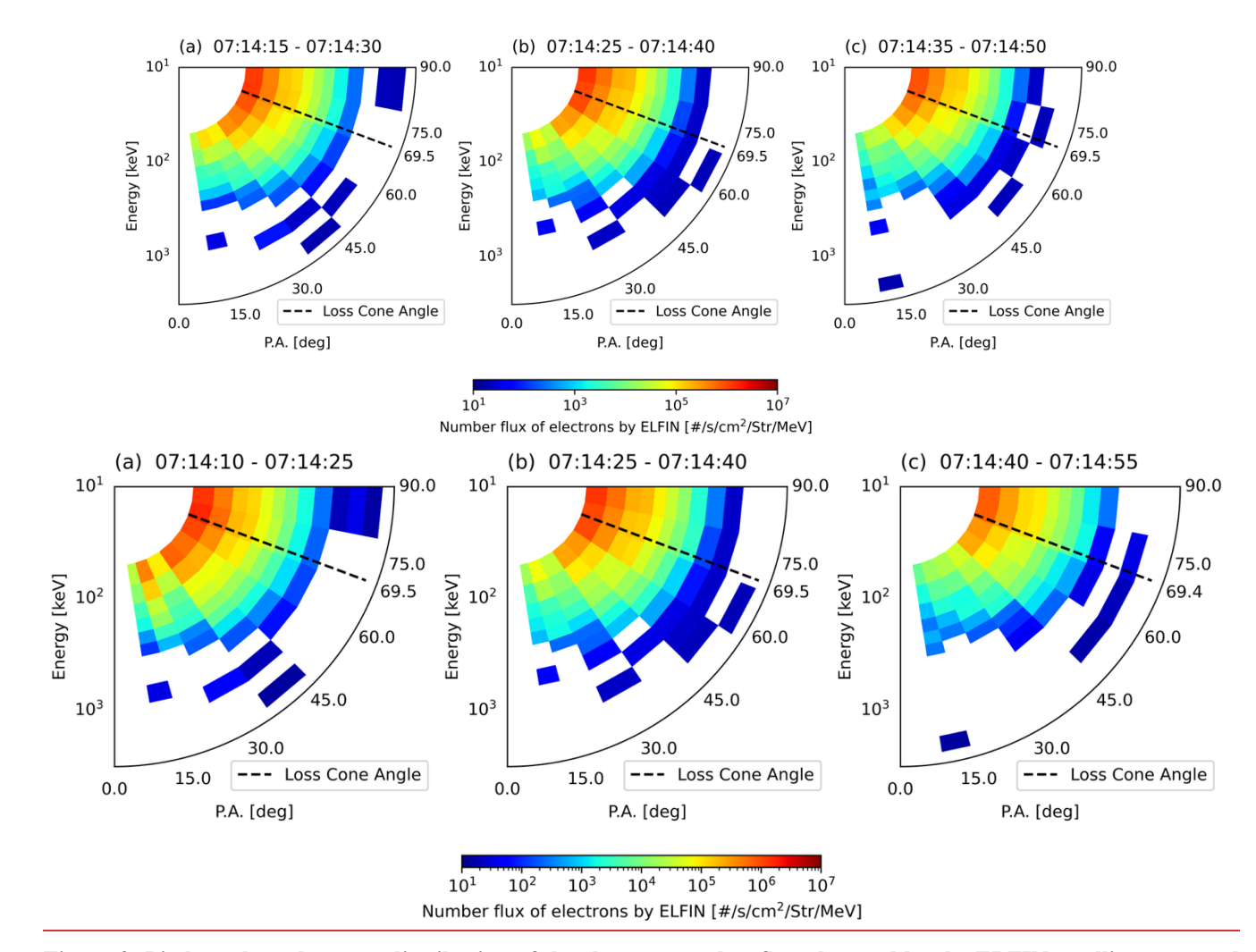


Figure 3: Pitch angle and energy distribution of the electron number flux observed by the ELFIN satellite, averaged during 15 s before (a), at the time (b), and after (c) the closest access of the satellite to the EISCAT Tromsø radar. Dashed lines indicate the loss cone angle.

3.1.3 Simulation results and comparison with EISCAT observation data

215

220

Figure 4 shows three types of altitude profiles of the electron density. The black line is the EISCAT Tromsø radar data, while the red and blue lines are simulated electron density using the electron distribution shown in Fig. 3(b) as an initial condition with and without the mirror force effect, respectively. Each peak value at 87 km altitude of the red and blue lines in Fig. 4 is made by 63 keV electrons, which is the minimum value of observed energy. Because electrons with energy less than 63 keV, out of observation, must have contributed to the atmospheric electron density above 87 km altitude, we compared the

simulation results to the radar data at altitudes below 85 km (see Zou et al., 2024). The density ratio between the simulations with and without the mirror force effect is 0.6 at 80 km altitude, and the value does not change significantly in the altitude range below 85 km. The altitude profile of electron density observed by the EISCAT radar at the same time is generally smaller than the values obtained from the two simulation results. The density ratio between the "with simulation" ("without simulation") and the EISCAT observation at 80 km is 1.7 (2.9), respectively. Hence, this result suggests that it might be important to consider the reduction in ionization due to the mirror force effect when studying ionization processes caused by EEP at altitudes below 85 km. it can be said that the mirror force effect is essential for studying the ionization process by the EEP at altitudes below 85 km.

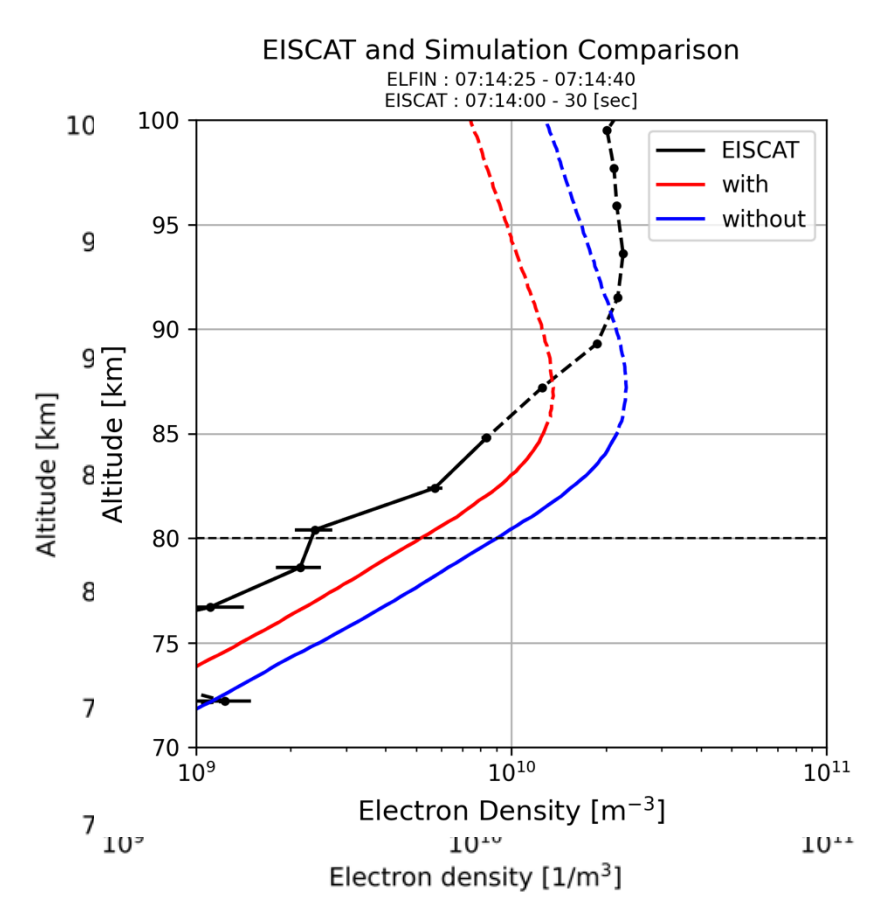


Figure 4: Altitude profile of electron density. Simulation results, with/without the mirror force effect, are shown by the red/blue lines, respectively. The black line shows the EISCAT Tromsø radar observation. Note that it is inappropriate to compare simulation results with the observed data above 85 km altitude because there must be an electron density enhancement due to lower energy electrons than observed by the ELFIN satellite.

3.24 The results of the other events and their characteristics

240

245

250

255

260

We investigated <u>fourfive</u> events, including the one described in Section 3. Table 1 <u>listshows</u> the date, <u>time</u>, <u>and MLT</u>, the density ratio at 80 km altitude. <u>The table also shows</u>, the energy flux percentage of trapped electrons, including boundary electrons (Tra. E-flux), <u>observed by the ELFIN satellite</u>, <u>and information on the aurora and AE index</u>. We calculated these values using <u>the</u> data of the time when the <u>ELFIN</u>-satellite was closest approach to the EISCAT Tromsø radar at the magnetic latitude of 66°.

Figure 5 shows a comparison between the EISCAT radar observations and the simulation results for all four events. The event on December 16, 2021 (the most right panel), showed that the EISCAT radar was able to derive more accurate altitude profile of electron density. For three of the events, the observed electron density agrees more closely with the simulation results with the mirror force than with those without the force, except for the event on 7 January. These results support taking the mirror force into account in calculations of electron density enhancement due to precipitating energetic electrons. On the other hand, the EISCAT radar did not observe a clear enhancement in electron density at low altitude on October 5, 2021, as would be expected based on the conjugate simulation result.

The density ratios <u>ranged fromwere between 0.5756 toand 0.807</u>. When the value was the smallest, (that was 0.5756) on <u>December 16, 2021</u>, trapped or boundary electrons accounted for <u>7280</u>% of the total energy flux. When the <u>ratio increased to value was the maximum of 0.80 on December 09, 2020</u>7, the energy flux carried by on the other hand, trapped or boundary electrons decreased tohad 35% of the total, energy flux, indicating a significant increase in the energy flux of electrons within the loss cone which is less than half of the former; thus, the pitch angle distribution was close to isotropic. Therefore, In addition, it was -10 min before the maxima of the horizontal geomagnetic component in Tromsø, and the peak of the AL decreased. Therefore, it was confirmed that the magnetic condition changed the pitch angle distribution, i.e., the density ratio if it was found that, as mentioned in Katoh et al. (2023), electrons with large pitch angles make a difference due to the mirror force, reducing the electron density in the atmosphere resulting from the actual distribution by approximately half (see Fig. 2) compared to the traditional method, which ignored the mirror force.

Focusing on whole events, the MLT distribution shows that differences due to the mirror force appear in the order of before midnight, at night, and in the morning. On the other hand, the AE index does not look like the key to the difference.

Table 1. Summary of conjunction events between the ELFIN satellite and EISCAT Tromsø radar

Date	UT	Density	Tra. E-
yy/mm/dd	MLT [hr]	ratio	flux
20/12/09	21:31 23.2	0.87	35%
21/01/07	19:52	0.65	93%

	21.5		
21/10/05	20:20 22.4	0.64	61%
21/11/27	07:36 9.9	0.56	80%
21/12/16	07:14 9.7	0.61	72%

270

EISCAT and Simulation Comparison

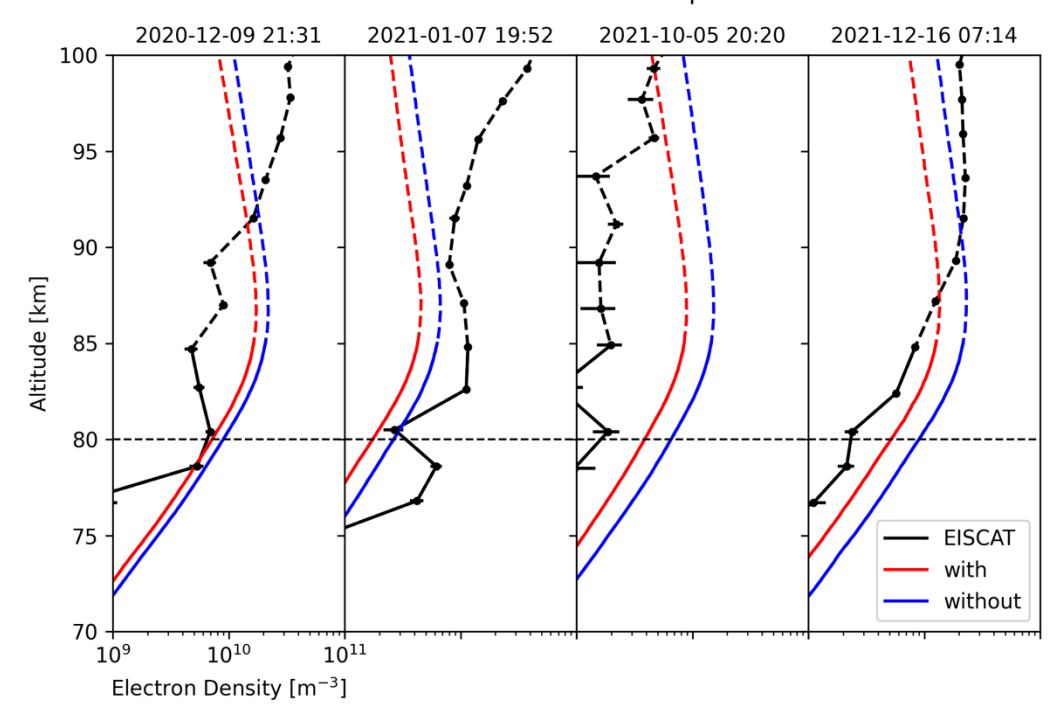
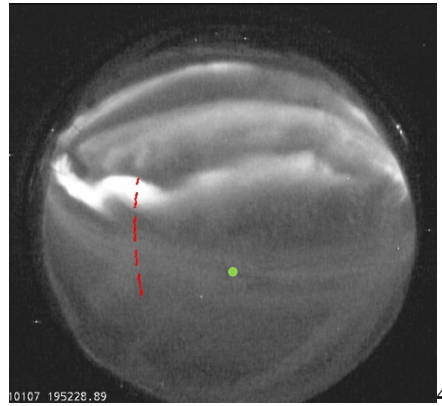


Figure 5: Electron density comparison between the EISCAT radar observation and simulations. The black lines are the observation results, and the red and blue lines indicate the simulation results with and without the mirror force, respectively.

Table 1. Summary of conjunction events between the ELFIN satellite and EISCAT Tromsø radar

<u>Date</u>	<u>UT</u>	Density ratio	<u>Tra. E-flux</u>
2020/12/09	21:31	0.80	<u>35%</u>
2021/01/07	<u>19:52</u>	0.66	93%
2021/10/05	20:20	0.59	<u>61%</u>
2021/12/16	07:14	0.57	<u>72%</u>



4 Discussion

285

density ratios at 80 km altitude with the MLT and the percentages of energy fluxes to identify the conditions under which differences due to the mirror force appeared. A value "pre/tra ratio" is the ratio of energy flux of precipitating electrons to trapped electrons. The MLT distribution of the pre/tra ratio was statistically analyzed with AE index classification (Qin et al., 2023; Tsai et al., 2024). Compared to the results of these studies, the results of our study were almost consistent with a larger proportion of pre/tra ratio in the order of before midnight, at night, and in the morning, as mentioned in the last section. In the 7 Jan. event, its value is out of trend, but that is because the percentage of boundary electrons energy flux was 50% and could not be meaningfully calculated. Although the images could not be analyzed in this study because

Table 1 A value "pre/tra ratio" is the ratio of energy flux of precipitating electrons to trapped electrons.compares the

they were unavailable, they seem related to the type of aurora. For instance, precipitating electrons from the radiation belt

- due to the wave-particle interaction are thought to have a relatively small pre/tra ratio because they originally had a large pitch angle to maintain the region. In fact, the density ratio was relatively small at 0.65 for the 7 Jan. event when the diffuse aurora was observed. In addition, the point that larger values of the AE index were associated with larger values of the pre/tra ratio is partly consistent with ours. In other words, the 16 Dec. event with 350 nT AE index in Fig 2f showed an increase in the pre/tra ratio along with the L value, which is consistent with the previous study.
- To compare the <u>overall</u> altitude profile of electron density, the simulation results and observational data <u>showedwere in</u> good agreement for the <u>December 16 December 2021</u> event (see <u>-section 3.2 and Fig. 54</u>), but not <u>necessarily clearly for</u> the other events. One of the reason for unclear comparison results in Fig. 5 is assumed to be the low signal-to-noise ratio of the electron density profile observed by the EISCAT Tromsø radar. It is known that the signal-to-noise ratio becomes significantly low when the electron density is less than 10¹⁰ [m⁻³], which has prevented accurate observation and comparison at an altitude of 80 km.
 - Another One of the reasons is mainly due to the spatial distance between the ELFIN satellite and the EISCAT Tromsø radar, but more accurate simulations are needed to compare its results to observational data, such as the introduction of secondary electrons. In detail, Fig. 4 also shows that the observed electron density was slightly lower than that calculated by the numerical simulation including the mirror force. This difference is most likely due to electrons scattered by whistler-mode waves (e.g., Zhang et al., 2023), as ed a minor disagreement between observation and simulation results. the event is characterized by intense bursty precipitations, most likely due to electrons scattered by whistler mode waves (e.g., Zhang et al., 2023). In that case, the electron flux is expected to vary on a time_-scales of seconds, but the satellite could not capture it within a limited latitude range conjugated to the radar.

310

- Additionally, the close timing of the observations does not necessarily indicate that the satellite and the radar observed the same precipitation event. As shown in Fig. 6, during the closest 15 seconds, the satellite footprint (red line) includes both discrete aurora and diffuse aurora, whereas the radar only observed the diffuse aurora region. Furthermore, as seen in Fig. 3, slight changes in latitude caused some variations in pitch angle and energy distributions. Therefore, small differences in the observed precipitation event may have led to discrepancies between the simulation and the observation results.
- Moreover, the difference in integration time between the two instruments (ELFIN: 15 seconds; EISCAT: 30 seconds) makes it even less certain that they observed the same precipitation. Neverthless, it is by chance that the conjunction event occurred during an EEP event. Since events where satellites and radars can closely observe the same region are difficult to capture, it is important to utilize other incoherent scatter radars, such as the PFISR (Poker Flat Incoherent Scatter Radar) in Alaska, to find additional events and validate the mirror force effect.

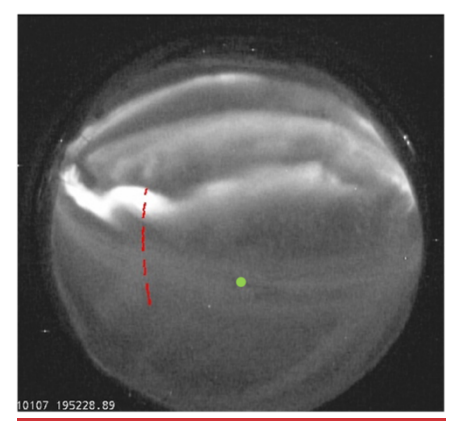


Figure 6: Optical data collected by at Tromsø on 7 January 2021. The red dashed line is the satellite footprint, and the green dot indicates the radar beam point.

The ionization profile during EEP is affected not only by pitch angle distribution but also by energy distribution. Katoh et al. (2023) found that the difference due to the consideration of the mirror force becomes more evident for electrons with higher energy. Additionally, the ratio-of trapped electrons always increase-decreases with energy when EEP occurs due to the whistler-mode waves (e.g., Tsai et al., 2023). Both results support the idea that higher energy electrons are more likely to be affected by the mirror force, which reduces the electron density in the atmosphere. On the other hand, it is known that the ratio sometimes remains constant for the 50-1000 keV range during intense precipitations by high-intensitye waves (Zhang et al., 2022) and that the ratio increases if precipitation is driven by EMIC waves (Capannolo et al., 2023). These studies suggest that the significance of the effect of the mirror force depends on the-wave strength or types, but we only found whistler-mode wave events in our conjugated observation. Therefore, it is necessary to statistically investigate the force's contribution to the electron density in the atmosphere with a focus on the type of wave.

In this study, we also examined the latitudinal distribution of the density ratio for only one event (see Fig. 2(g)). We found that the difference due to the mirror force depends on the latitude and that the ratio is more likely to be smaller as the latitude decreases low, even while electrons seemed to be precipitating from the radiation belt. This is because the distribution of electrons depends on the latitude. Specifically, this is because the percentage of trapped electrons was more significant at lower latitudes. It is also statistically consistent with Qin's finding that the smaller the L value, the larger the ratio of smaller the pre/tra energy flux of trapped electrons ratio. However, the effects of the mirror force, i.e., the variations in density ratios due to distribution changes in both the energy and pitch angle, are not yet fully understood, so more ELFIN satellite observation events should be used to examine the latitudinal distribution of the ratio.

Finally, this study focused on the magnetic mirror force and included its effects in the simulation to see how it changes the electron density enhancement in the atmosphere. It was mentioned in Katoh et al. (2023) that some electrons move back toward away from the atmosphere, i.e., go up again. However, even though the ELFIN satellite observed the flux of upgoing electrons, a comparison between the observational data and the simulation results has yet to be made. In the future, it can be

verified whether the upgoing electrons observed would be consistent with the simulation results by improving the simulation code so that the energy and pitch angle distributions of the reflected electrons can be calculated.

5 Conclusion

350 This study aims to evaluate the effect of the mirror force on precipitating electrons and, consequently, atmospheric electron density by focusing on the pitch angle of the electrons. We used ELFIN satellite data and a simulation developed by Katoh et al. (2023). We found that the electron density due toby EEP can be about 40% smaller when the effect of the mirror force is considered than when ithe result ignored the effect as in previous studies (e.g., Murase et al., 2023). The simulation results were compared with simultaneous data from with the EISCAT Tromsø radar. For an event where the altitude profile of electron 355 density was accurately determined from the EISCAT radar on December 16, 2021, the simulated electron density profile, including the mirror force effect, is closer to the actual density profile from EISCAT than when ignoring the effect. The result was validated using the EISCAT Tromsø radar; the simulated electron density, including the effect, is closer to the actual value than ignoring it. Furthermore, although this is not a conjunction event between the ELFIN satellite and the radar, some pitch angle distribution made the ratio reach 50% at maximum. In other words, these results suggest the importance of considering 360 the pitch angle distribution of electrons and the effect of EEP on the simulation of electron density enhancement in the atmosphere, or the result wwould differ by about 50%get half of the error value. Additionally, in order to accurately estimate the effects of atmospheric ionisation, it is desirable for electron instruments with Low Earth Orbit (LEO) satellites to observe pitch angle distributions with high resolution, which can distinguish between trapped and precipitating particles. In addition, satellite electron observations at low altitudes should observe pitch angle distributions with high resolution that can at least 365 distinguish trapped or precipitating particles.

Author contributions

370

Y. O. designed this study. Y. K. instructed T. T. on the use of simulation he developed. A. A., V. A., and X. Z., collected and proceeded the data observed by the ELFIN satellites. Y. O., Y. K., A. K., Y. T., and M. F. supervised the work. M. F. and T. T. analysed the data. T. T. made the figures and drafted the manuscript. All authors discussed the results and approaved the manuscript.

Acknowledgments

This research was supported by the Grants-in-Aid for Scientific Research (20K04052, 20KK0313, and 23H05429) by the 375 Ministry of Education, Science, Sports and Culture, Japan.

References

395

- Alken, P., Thébault, E., Beggan, C.D. et al.: International Geomagnetic Reference Field: the thirteenth generation. Earth Planets Space 73, 49, https://doi.org/10.1186/s40623-020-01288-x, 2021.
- Angelopoulos, V., Tsai, E., Bingley, L., Shaffer, C., Turner, D. L., Runov, A., Li, W., Liu, J., Artemyev, A. V., Zhang, X.-J.,
 Strangeway, R. J., Wirz, R. E., Shprits, Y. Y., Sergeev, V. A., Caron, R. P., Chung, M., Cruce, P., Greer, W., Grimes, E.,
 Hector, K., Lawson, M. J., Leneman, D., Masongsong, E. V., Russell, C. L., Wilkins, C., Hinkley, D., Blake, J. B., Adair,
 N., Allen, M., Anderson, M., Arreola-Zamora, M., Artinger, J., Asher, J., Branchevsky, D., Capitelli, M. R., Castro, R.,
 Chao, G., Chung, N., Cliffe, M., Colton, K., Costello, C., Depe, D., Domae, B. W., Eldin, S., Fitzgibbon, L., Flemming,
 A., Fox, I., Frederick, D. M., Gilbert, A., Gildemeister, A., Gonzalez, A., Hesford, B., Jha, S., Kang, N., King, J., Krieger,
 R., Lian, K., Mao, J., McKinney, E., Miller, J. P., Norris, A., Nuesca, M., Palla, A., Park, E. S. Y., Pedersen, C. E., Qu,
 Z., Rozario, R., Rye, E., Seaton, R., Subramanian, A., Sundin, S. R., Tan, A., Turner, W., Villegas, A. J., Wasden, M.,
 Wing, G., Wong, C., Xie, E., Yamamoto, S., Yap, R., Zarifian, A., and Zhang, G. Y.: The ELFIN Mission, Space Sci
 Rev, 216, 103, https://doi.org/10.1007/s11214-020-00721-7, 2020.
- Capannolo, L., Li, W., Ma, Q., Qin, M., Shen, X.-C., Angelopoulos, V., Artemyev, A., Zhang, X.-J., and Hanzelka, M.:

 Electron Precipitation Observed by ELFIN Using Proton Precipitation as a Proxy for Electromagnetic Ion Cyclotron (EMIC) Waves, Geophysical Research Letters, 50, e2023GL103519, https://doi.org/10.1029/2023GL103519, 2023.

CelesTrak. https://celestrak.org/SpaceData/

- Emmert, J. T., Drob, D. P., Picone, J. M., Siskind, D. E., Jones Jr., M., Mlynczak, M. G., Bernath, P. F., Chu, X., Doornbos, E., Funke, B., Goncharenko, L. P., Hervig, M. E., Schwartz, M. J., Sheese, P. E., Vargas, F., Williams, B. P., and Yuan, T.: NRLMSIS 2.0: A Whole Atmosphere Empirical Model of Temperature and Neutral Species Densities, Earth and Space Science, 8, e2020EA001321, https://doi.org/10.1029/2020EA001321, 2021.
- Emmert, J. T., Jones Jr, M., Siskind, D. E., Drob, D. P., Picone, J. M., Stevens, M. H., Bailey, S. M., Bender, S., Bernath, P. F., Funke, B., Hervig, M. E., and Pérot, K.: NRLMSIS 2.1: An Empirical Model of Nitric Oxide Incorporated Into MSIS, Journal of Geophysical Research: Space Physics, 127, e2022JA030896, https://doi.org/10.1029/2022JA030896, 2022.
- Folkestad, K., Hagfors, T., and Westerlund, S.: EISCAT: An updated description of technical characteristics and operational capabilities, Radio Science, 18, 867–879, https://doi.org/10.1029/RS018i006p00867, 1983.
 - Gledhill, J. A.: The effective recombination coefficient of electrons in the ionosphere between 50 and 150 km, Radio Science, 21, 399–408, https://doi.org/10.1029/RS021i003p00399, 1986.

- Katoh, Y., Rosendahl, P. S., Ogawa, Y., Hiraki, Y., and Tadokoro, H.: Effect of the mirror force on the collision rate due to energetic electron precipitation: Monte Carlo simulations, Earth Planets Space, 75, 117, https://doi.org/10.1186/s40623-023-01871-y, 2023.
 - Lehtinen, M., and A. Huuskonen (1996), General incoherent scatter analysis and GUISDAP, J. Atmos. Terr. Phys., 58(1), 435–452, doi:10.1016/0021-9169(95)00047-X.
- Lehtinen, N. G., Bell, T. F., and Inan, U. S.: Monte Carlo simulation of runaway MeV electron breakdown with application to red sprites and terrestrial gamma ray flashes, Journal of Geophysical Research: Space Physics, 104, 24699–24712, https://doi.org/10.1029/1999JA900335, 1999.
 - Lucas, G. (2022). pymsis [Computer software]. doi:10.5281/zenodo.5348502
 - Matzka, J., Stolle, C., Yamazaki, Y., Bronkalla, O., and Morschhauser, A.: The Geomagnetic Kp Index and Derived Indices of Geomagnetic Activity, Space Weather, 19, e2020SW002641, https://doi.org/10.1029/2020SW002641, 2021.
- Miyoshi, Y., Saito, S., Kurita, S., Asamura, K., Hosokawa, K., Sakanoi, T., Mitani, T., Ogawa, Y., Oyama, S., Tsuchiya, F., Jones, S. L., Jaynes, A. N., and Blake, J. B.: Relativistic Electron Microbursts as High-Energy Tail of Pulsating Aurora Electrons, Geophysical Research Letters, 47, e2020GL090360, https://doi.org/10.1029/2020GL090360, 2020.
 - Miyoshi, Y., Hosokawa, K., Kurita, S. *et al.* Penetration of MeV electrons into the mesosphere accompanying pulsating aurorae. *Sci Rep* 11, 13724, https://doi.org/10.1038/s41598-021-92611-3, 2021.
- Murase K, Kataoka R, Nishiyama T, Nishimura K, Hashimoto T, et al.: Mesospheric ionization during substorm growth phase. J. Space Weather Space Clim. 12, 18, https://doi.org/10.1051/swsc/2022012, 2022.
 - Murase, K., Kataoka, R., Nishiyama, T., Sato, K., Tsutsumi, M., Tanaka, Y., Ogawa, Y., and Sato, T.: Atmospheric Ionizations by Solar X-Rays, Solar Protons, and Radiation Belt Electrons in September 2017 Space Weather Event, Space Weather, 21, e2023SW003651, https://doi.org/10.1029/2023SW003651, 2023.
- Nesse Tyssøy, H., Sinnhuber, M., Asikainen, T., Bender, S., Clilverd, M. A., Funke, B., van de Kamp, M., Pettit, J. M., Randall, C. E., Reddmann, T., Rodger, C. J., Rozanov, E., Smith-Johnsen, C., Sukhodolov, T., Verronen, P. T., Wissing, J. M., and Yakovchuk, O.: HEPPA III Intercomparison Experiment on Electron Precipitation Impacts: 1. Estimated Ionization Rates During a Geomagnetic Active Period in April 2010, Journal of Geophysical Research: Space Physics, 127, e2021JA029128, https://doi.org/10.1029/2021JA029128, 2022.
- Oyama, S., Kero, A., Rodger, C. J., Clilverd, M. A., Miyoshi, Y., Partamies, N., Turunen, E., Raita, T., Verronen, P. T., and Saito, S.: Energetic electron precipitation and auroral morphology at the substorm recovery phase, Journal of Geophysical Research: Space Physics, 122, 6508–6527, https://doi.org/10.1002/2016JA023484, 2017.
 - Ozaki, M., Shiokawa, K., Kataoka, R. *et al.* Localized mesospheric ozone destruction corresponding to isolated proton aurora coming from Earth's radiation belt. *Sci Rep* **12**, 16300, https://doi.org/10.1038/s41598-022-20548-2, 2022.
- 435 Picone, J. M., Hedin, A. E., Drob, D. P., and Aikin, A. C.: NRLMSISE 00 empirical model of the atmosphere: Statistical comparisons and scientific issues, Journal of Geophysical Research: Space Physics, 107, SIA 15-1 SIA 15-16, https://doi.org/10.1029/2002JA009430, 2002.

Qin, M., Li, W., Shen, X.-C., Angelopoulos, V., Selesnick, R., Capannolo, L., Ma, Q., Artemyev, A., and Zhang, X.-J.: Global Survey of Energetic Electron Precipitation at Low Earth Orbit Observed by ELFIN, Geophysical Research Letters, 51, e2023GL105134, https://doi.org/10.1029/2023GL105134, 2024.

440

- Rees, M. H.: Auroral ionization and excitation by incident energetic electrons, Planetary and Space Science, 11, 1209–1218, https://doi.org/10.1016/0032-0633(63)90252-6, 1963.
- Sergeev V, Nishimura Y, Kubyshkina M, Angelopoulos V, Nakamura R, Singer H. 2012. Magnetospheric location of the equatorward prebreakup arc. J Geophys Res 117: A01212. https://doi.org/10.1029/2011JA017154.
- Solomon, S. C.: auroral electron transport using the Monte Carlo Method, Geophysical Research Letters, 20, 185–188, https://doi.org/10.1029/93GL00081, 1993.
 - Solomon, S. C.: Auroral particle transport using Monte Carlo and hybrid methods, Journal of Geophysical Research: Space Physics, 106, 107–116, https://doi.org/10.1029/2000JA002011, 2001.
- Tsai, E., Artemyev, A., Anglelopoulos, V., and Zhang, X.-J.: Investing Whistler-Mode Intensity Along Field Lines Using
 Electron Precipitation Measurements, Journal of Geophysical Research: Space Physics, 128, e2023JA031578, https://doi.org/10.1029/2023JA031578, 2023.
 - Tsai, E., Artemyev, A., Ma, Q., Mourenas, D., Agapitov, O., Zhang, X.-J., and Angelopoulos, V.: Key Factors Determining Nightside Energetic Electron Losses Driven by Whistler-Mode Waves, Journal of Geophysical Research: Space Physics, 129, e2023JA032351, https://doi.org/10.1029/2023JA032351, 2024.
- 455 <u>Turunen, E., P. T. Verronen, A. Seppälä, C. J. Rodger, M. A. Clilverd, J. Tamminen, C.-F. Enell, and T. Ulich (2009), Impact of different energies of precipitating particles on NOx generation in the middle and upper atmosphere during geomagnetic storms, J. Atmos. Sol. Terr. Phys., 71, 1176–1189, https://doi.org/10.1016/j.jastp.2008.07.005.</u>
 - Turunen, E., Kero, A., Verronen, P. T., Miyoshi, Y., Oyama, S.-I., and Saito, S.: Mesospheric ozone destruction by high-energy electron precipitation associated with pulsating aurora, Journal of Geophysical Research: Atmospheres, 121, 11,852-11,861, https://doi.org/10.1002/2016JD025015, 2016.
 - Xu, W., Marshall, R. A., Tyssøy, H. N., and Fang, X.: A Generalized Method for Calculating Atmospheric Ionization by Energetic Electron Precipitation, Journal of Geophysical Research: Space Physics, 125, e2020JA028482, https://doi.org/10.1029/2020JA028482, 2020.
- Zhang, X.-J., Angelopoulos, V., Mourenas, D., Artemyev, A., Tsai, E., and Wilkins, C.: Characteristics of Electron Microburst

 Precipitation Based on High-Resolution ELFIN Measurements, Journal of Geophysical Research: Space Physics, 127,
 e2022JA030509, https://doi.org/10.1029/2022JA030509, 2022.
 - Zhang, X.-J., Angelopoulos, V., Artemyev, A., Mourenas, D., Agapitov, O., Tsai, E., Wilkins, C.: Temporal Scales of Electron Precipitation Driven by Whistler-Mode Waves, Journal of Geophysical Research: Space Physics, 128, e2022JA031087, https://doi.org/10.129/2022JA031087, 2023.

470 Zou, Y., Zhang X.-J., Artemyev, A., Shen, Y., and Angelopoulos, V.: The Key Role of Magnetic Curvature Scattering in Energetic Electron Precipitation During Substorm, Journal of Geophysical Research Letters, 51, e2024GL109227, https://doi.org/10.1029/2024GL109227, 2024.